Since January 2020 Elsevier has created a COVID-19 resource centre with free information in English and Mandarin on the novel coronavirus COVID-19. The COVID-19 resource centre is hosted on Elsevier Connect, the company's public news and information website.

Chinese Journal of Mechanical Engineering: Additive Manufacturing Frontiers 1 (2022) 100025

Contents lists available at ScienceDirect

Chinese Journal of Mechanical Engineering: Additive Manufacturing Frontiers

journal homepage: www.elsevier.com/locate/cjmeamf

Construction and Application of *in vitro* Alveolar Models Based on 3D Printing Technology

Tiankun Liu[a,b,1], Chang Zhou[a,b,1], Yongchun Shao[a,b], Zhuo Xiong[a,b], Ding Weng[c,*], Yuan Pang[a,b,*], Wei Sun[a,b,d]

[a] *Department of Mechanical Engineering, Biomanufacturing Center, Tsinghua University, Beijing, 100084, China*
[b] *Biomanufacturing and Rapid Forming Technology Key Laboratory of Beijing, Beijing, 100084, China*
[c] *State Key Laboratory of Tribology, School of Mechanical Engineering, Tsinghua University, Beijing, 100084, China*
[d] *Department of Mechanical Engineering, Drexel University, Philadelphia, PA 19104, USA*

ARTICLE INFO

Keywords:
3D printing
Lung model
Hydrogel beads
Microcapsule
Toxicity test

ABSTRACT

Increasing lung diseases, mutating coronaviruses, and the development of new compounds urgently require biomimetic *in vitro* lung models for lung pathology, toxicology, and pharmacology. The current construction strategies for lung models mainly include animal models, 2D cell culture, lung-on-a-chip, and lung organoids. However, current models face difficulties in reproducing *in vivo*-like alveolar size and vesicle-like structures, and are unable to contain multiple cell types. In this study, a strategy for constructing alveolar models based on degradable hydrogel microspheres is proposed. Hydrogel microspheres, 200–250 μm in diameter, were prepared using a self-developed printing technique driven by alternating viscous and inertial forces. Microcapsules were further constructed using a coacervation-based layer-by-layer technique and core liquefaction. Three types of cells were inoculated and co-cultured on hydrogel capsules based on optimized microcapsule surface treatment strategies. Finally, an *in vitro* three-dimensional endothelial alveolar model with a multicellular composition and vesicle-like structure with a diameter of approximately 230 μm was successfully constructed. Cells in the constructed alveolar model maintained a high survival rate. The LD_{50} values of glutaraldehyde based on the constructed models were in good agreement with the reference values, validating the potential of the model for future toxicant and drug detection.

1. Introduction

The lung is an important respiratory organ in the human body that allows exchange of gas between internal tissues and the external environment. The alveolus, the functional unit of lung organs, is the main site of gas exchange. The alveoli in the body appear as spherical sacs with diameter of 200–250 μm [1]. The alveolar wall consists of a single layer of epithelial cells, which consists of type I and type II alveolar epithelial cells (Fig. 1(a)) [2]. The interstitial space of adjacent alveoli is enriched with connective tissues, including the capillary network [3], elastic fibers, reticular fibers, and collagen fibers, which promote adequate gas exchange between the alveoli and blood in the capillaries. A wide surface area, thin alveolar wall structure, and rich vascular network provide an adequate and open area for gas exchange [2]. However, these characteristics also lead to rapid absorption of volatile liquids, aerosols, solid particles, and disease-causing microorganisms, making the lungs susceptible to various harmful substances. Lung diseases are becoming increasingly common and pose a serious threat to human health [4]. Chronic obstructive pulmonary disease [5] and lower respiratory infections were ranked 3rd and 4th, respectively, among the top ten causes of death worldwide in 2016, and the 2019 corona virus disease (COVID-19) is currently responsible for nearly $10 trillion economic losses worldwide. Facing the increasingly critical lung disease situation [6–8], a biomimetic lung model is urgently needed for pathology researchers and rapid toxicity tests.

Conventional animal models and two-dimensional (2D) cell cultures have been used to construct lung models. Animal models are still the most commonly used lung models and are important references for clinical testing of drugs [9]. They can reflect the effects of drugs at the individual level, but still face challenges including high costs, long cycles, species differences, and deviations in drug effectiveness and safety test results [10]. *In vitro* 2D models use Petri dishes to construct single-layer planar cultured lung models [11] that are convenient in operation and short in culture cycle, but are unable to stimulate the mechanical and functional properties of the cell microenvironment [12]. With the advancement of culture methods, 2.5D models based on transwell

* Corresponding authors.
E-mail addresses: dingweng@tsinghua.edu.cn (D. Weng), pangyuan31@tsinghua.edu.cn (Y. Pang).
[1] These Authors contribute to this work equally.

https://doi.org/10.1016/j.cjmeam.2022.100025
Received 8 January 2022; Received in revised form 6 May 2022; Accepted 7 May 2022
Available online 16 June 2022

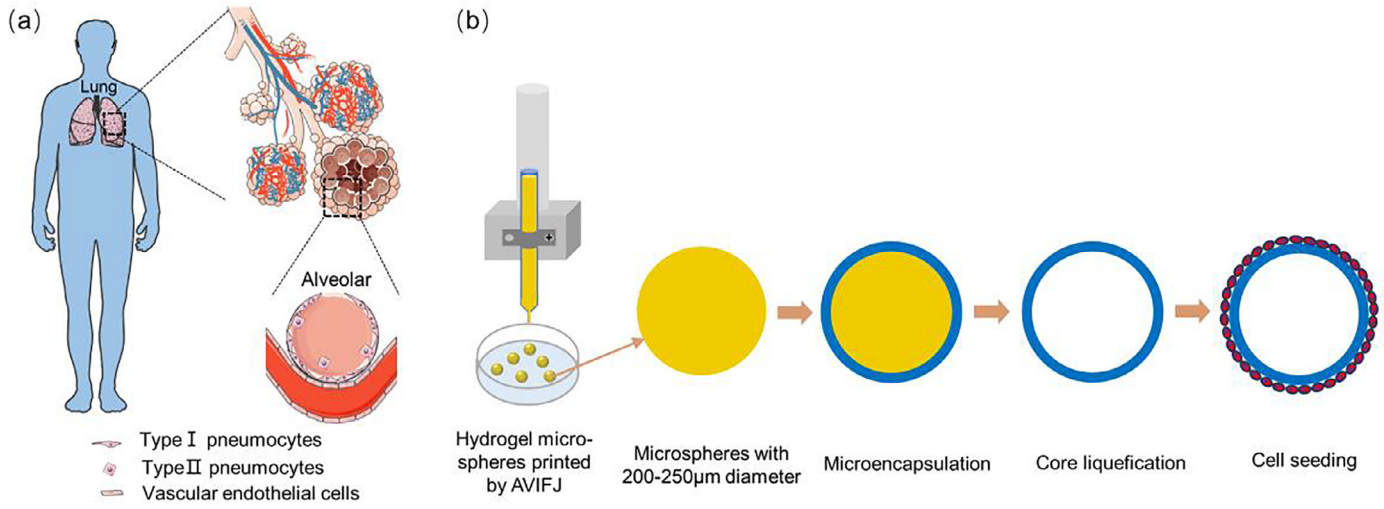

Fig. 1. Design concept and construction process of alveolar model: (a) Illustration of human alveolar tissue; (b) Roadmap of *in vitro* construction of alveolar model based on alternating viscous and inertial forces jetting (AVIFJ) technology.

can now simulate the air-blood barrier via air-liquid interface cultures [13], contain complex cell composition via co-culture of alveolar epithelium, immune cells, and endothelial cells [14], and construct high-throughput systems via batch manufacturing [15]. Despite the improvement of the model in terms of biomimetics, the conventional transwell can only achieve a controlled arrangement of cells in a single layer and cannot simulate the real alveolar tissue structure and cell distribution [16].

Unlike 2D and transwell models, three-dimensional (3D) lung models are expected to reproduce the characteristic lung tissue structure and simulate 3D cell-cell interactions. In addition, the designed scaffold and cellular arrangement are expected to better simulate the diffusion gradients of oxygen, nutrients, cellular metabolites, and toxic drug effects. Decellularized scaffolds retain both the microscopic and macroscopic structures of the lung, as well as the components of the extracellular matrix [17], and provide a more physiological setting for studying human lung diseases [18]. However, the complex processing steps during scaffold preparation may have side effects on cell binding, survival, and proliferation during recellularization. High costs, limited sources, and ethical issues are also challenges for decellularized lung scaffolds. Lung chips are microfluidic chip-based cell culture devices containing multiple chambers with continuous perfusion [19,20], and can more effectively simulate multicellular structures, interfaces, physicochemical microenvironments, and blood perfusion [21,22]. Huh et al. constructed a lung chip model capable of simulating the gas-blood barrier and respiratory stress [23]. Zhang et al. used a similar lung chip to create a novel coronavirus infection model. This model reproduces the lung injury, immune response, and drug responses at the organ level, providing a unique platform for COVID-19 pathology studies and drug development [24]. However, polydimethylsiloxane (PDMS) materials commonly used in microfluidic chips have protein adsorption properties, which affect the accuracy of drug effects [25,26]. The planar structure constructed by the microfluidic chip cannot simulate the spherical or curved structure of alveolar tissue. Organoids are organ-specific multicellular 3D cultures developed from different types of stem cells [7,27], and are capable of achieving some of the key structural and functional properties of the corresponding organs [28]. However, organoid structures lack vascular networks, immune cells, and other important substrates that form hollow alveolar structures [29]. The long preparation time, poor homogeneity, and oversensitivity to the external environment also pose challenges for the preparation of organoid models.

To date, there is still a gap between the constructed lung models and tissues in terms of cell constituents, alveolar microstructure, and drug screening. The alveolar wall is composed of multiple epithelial cells and is in contact with several endothelial cells and fibroblasts, which play important roles in physiological, toxicological, and pharmacological studies. Most current lung models are constructed based on a single species of lung epithelial cells with low cellular composition complexity. To further integrate the tissue into an efficient and accurate drug screening platform, a biomimetic alveolar structure must also be constructed. There is growing evidence that the radius of curvature and surface in the near-cellular range affect cell behavior [30–32]. The 200–250 μm spherical structure increases the surface area of the alveoli and guarantees high material exchange efficiency [32]. However, most current lung models are unable to simulate a spherical alveolar structure with characteristic sizes [33]. Finally, despite the great interest in drug delivery via the pulmonary route in the last few years, clinical animal models still suffer from first-pass effects and low enrichment in the lungs, failing to reasonably recapitulate the characteristic lung pathology [34,35]. An *in vitro* alveolar model with multicellular composition and topology mimicry of 200 μm microcapsules applied to drug screening will hopefully complement existing models, expand the current understanding in the field, and work as a proof of concept for a more complex and biomimetic alveolar model.

Based on these urgent needs, this study aims to construct a 3D biomimetic alveolar model that can simulate the alveolar microstructure and multicellular composition to provide more accurate detection results for the evaluation of toxicants. Alveolar epithelial and endothelial cells adhere to gel microcapsules with liquefied cores constructed by 3D printing to mimic the real alveolar morphology *in vivo* (Fig. 1(b)). Based on a novel 3D printing technology named alternating viscous and inertial forces jetting (AVIFJ) and a sodium alginate material, we first realized the controllable preparation of hydrogel microspheres (MSs) with a diameter of 230 μm. The alveolar-like microcapsule structures were realized via layer-by-layer coalescence and core liquefaction. The surface treatment improved cell adhesion and finally realized the construction of a spherical alveolar model with a multicellular composition, endothelialization, and diameter of approximately 230 μm. Biological evaluation and toxicity tests were carried out based on the constructed models, and the results showed that the cells in the model maintained high cell viability and consistency with the current reference data.

2. Materials and Methods

2.1. Cell culture

A549 human adenocarcinoma cells (CCL-185) were purchased from the American type culture collection (ATCC) and cultured in Dulbecco's

modified Eagle's medium (DMEM, Gibco) containing 10% fetal bovine serum (FBS, Hyclone), 1% penicillin/streptomycin (100 U/mL, BI), 1% GlutaMAX (Gibco), and 1% nonessential amino acids (NEAA, Gibco). Human umbilical vein endothelial cells (HUVECs) purchased from ATCC were cultured in DMEM (Gibco, 11965092). NIH-3T3 cells purchased from ATCC were cultured in the same medium as the A549 cells.

2.2. Material preparation

Sodium alginate powder (A0682, Sigma) was dissolved in 0.9% saline to obtain alginate solutions with concentrations of 1%, 2%, 3%, and 4% weight per volume (w/v). A magnetic stirrer was used to accelerate the dissolution of sodium alginate at 40 ˚C. 0.5 g of chitosan powder was dissolved in 2% (w/v) glacial acetic acid solution and kept at 40 ˚C overnight to form a transparent 1% chitosan solution. The pH of the solution was further adjusted to 7.0 by adding 0.1 mol/L NaOH. The above solution was sterilized via heating in an oven (70 ˚C) three times. $CaCl_2$ powder was dissolved in deionized water to a concentration of 3% (w/v). The solution was sterilized by being pushed through a 0.22 μm filter membrane before use. The viscosity of the alginate solution was further tested using an Anton Paar rheometer (MCR 304, Austria). Viscosity data point information was collected at an appropriate time interval, and all data were subsequently collected into a diagram and analyzed.

2.3. Nozzle preparation

The preparation of the AVIFJ nozzle was described in previously published articles [36]. Briefly, the nozzle was fabricated by pulling glass micropipettes (BF 150-110-10; Sutter, USA) with a puller (P-1000; Sutter, USA). A micro-forge needle instrument (MF-900, Narishige, Japan) was used to cut the needle to a designated caliber.

2.4. Hydrogel MSs printing by AVIFJ

A self-developed AVIFJ printing system was used in this experiment, and its printability was comprehensively introduced previously [37]. Before printing, the 2% sodium alginate solution was pushed into the nozzle through a silicone hose using a 1 mL syringe. A 2 mL $CaCl_2$ solution in a 35 mm untreated Petri dish was used to crosslink the droplets. The vibration period, amplitude, and amplifier magnification parameters of the printing process were set to 0.2 s, 10 V, and 15, respectively. After printing, the Petri dish was left to stand for 5 min to fully crosslink the alginate MSs.

2.5. Microcapsules constructing by microencapsulation

Microcapsules constructed from MSs are based on cationic ion polymerization and core liquefaction technology. After printing, the MS suspension was centrifuged at 7 g for 1 min and rinsed twice with 0.9% normal saline. Subsequently, MSs were resuspended in 1% chitosan solution and kept on a shaker for 20 min. After centrifuging and rinsing again, the MSs were resuspended in 1% sodium alginate solution and placed on a shaker for 20 min. By repeating the above-mentioned chitosan coating process, a three-layered structure of chitosan-alginate-chitosan was constructed on the outer surface of the MSs.

A 2.5% volume per volume (v/v) red fluorescent particle (R0100, Thermo Fisher) was added to the 2% sodium alginate solution to better illustrate the liquefaction inside the MSs. After the MSs were encapsulated, they were washed twice with a sodium chloride solution and resuspended in a 1% sodium citrate solution. Subsequently, the MSs were transferred to 35 mm Petri dishes, placed on a shaker for 40 min, and processed for 5 min to liquefy the alginate in the core. To confirm the liquefied core in the microcapsules, the microcapsules were observed under a confocal microscope in a long-time dynamic observation mode.

2.6. Surface treatment of microcapsules and cell attachment

The sterilized 2% sodium alginate solution was mixed with a 4 mg/mL rat tail type I collagen solution in a 3:1 ratio to form an alginate-collagen polymerization solution. The rat tail type I collagen solution was diluted to 1 mg/mL with sterile saline. A polylysine solution (Beijing Reagan, ih0095, 10 × PLL, 1 mg/mL) was diluted to 20 μg/mL using sterile saline. The microcapsules were coated with four different treatments: (a) coating the mixture of alginate and collagen onto the MS surface; (b) coating alginate first and then collagen; (c) coating alginate first and then chitosan, and (d) coating alginate first and then polylysine. After treatment, 5×10^5 cells/mL A549 and 6000 spheres/mL microcapsules were mixed in the ratio of 1:1 and co-cultured in a low-adherent six-well plate.

2.7. Multicellular seeding on microcapsules

To facilitate the observation of cellular distribution, Celltracker™ Green CMFDA and Red CMTPX (Invitrogen, c34552) were used to stain A549 cells and HUVECs, respectively, following the manufacturer's instructions. Before seeding, A549, HUVECs, and 3T3 cells were digested and resuspended to a cell density of 5×10^5 cells/mL. The concentration of microcapsules was 5000/mL, and A549, HUVECs, and 3T3 cells were co-cultured in the ratio of 9:9:2 in a PDMS-based microwell device following previously established protocols [38,39]. Honeycomb microwell arrays of diameter 326 μm were prepared by casting PDMS on silicon wafers. The resulting PDMS membrane was peeled off, treated with hydrophobic agents, cut, and fixed in a 24-well culture plate for cell inoculation. The cells and microcapsules were cultured for 2 days before conducting the follow-up experiments.

2.8. Live/dead staining assay

The calcein-AM/PI double staining kit (C542) was purchased from Dojindo, Japan. The live/dead staining work solution was added to a 15 mL tube to resuspend the alveolar models, followed by incubation on a shaker for 20 min and imaging using a confocal microscope. The image stacks were analyzed for live(green)/dead(red) cell rates using Image Pro-plus 7.0.

2.9. Toxicity assay

A 50% glutaraldehyde solution was added to the alveolar models surrounded by the three types of cells to a final concentration of 0, 100, 200, 400, 500, and 750 ng/mL. The alveolar models were placed on a shaker in an incubator and cultured at 30 r/min at 37 ˚C for 4 h. After treatment, the cells were stained with a live/dead assay solution as described above, and then observed under a confocal fluorescence microscope.

2.10. Statistical analysis

Statistical analysis and curve drawing were performed using Microsoft Excel (Microsoft, USA). All data are presented as mean ± standard deviation.

3. Results and Discussion

3.1. Printability of sodium alginate MSs by AVIFJ

The AVIFJ utilizes alternating viscous and inertial forces during vibrations to generate droplets. Although the printing process is gentle, the limited drive may hinder the range of printed biomaterials, particularly hydrogels with high viscosity. The viscosities of different concentrations of sodium alginate solution (1%, 2%, 3%, and 4%) were first

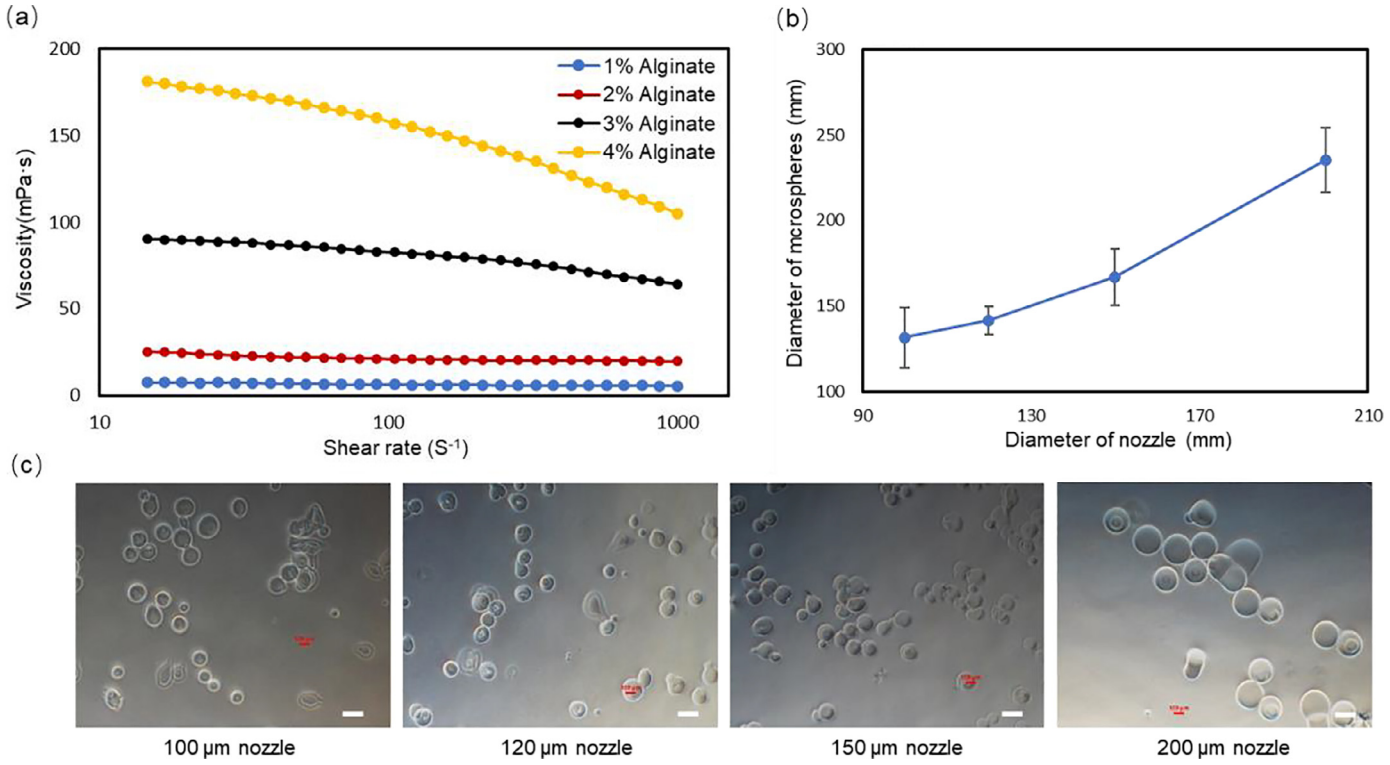

Fig. 2. Printability of alginate by AVIFJ and printed MS: (a) Viscosity of different concentration of sodium alginate solution; (b) Relevance curve between the size of printed hydrogel microspheres and the diameter of nozzles; (c) Printed hydrogel microspheres under microscopic observation (Scale bar: 200 μm).

tested, as shown in Fig. 2(a). Considering the steep increase in viscosity when the concentration exceeded 2%, 2% sodium alginate solution was selected for printing. The diameter of the glass microneedle tip is also an important parameter for determining the size of hydrogel MSs. The relationship between the size of MSs and the diameter of the microneedles is shown in Fig. 2(b). The diameter of the microneedle used for printing MSs with diameters of 230.927 ± 19.090 μm ($^{**}P < 0.01$) was 180 μm, satisfying the printing requirements of 200–250 μm MSs. The 2% concentration of alginate MSs printed by the different diameters of the microneedles shown in Fig. 2(c) reveals good forming stability. The optimized 2% sodium alginate solution and 180 μm diameter microneedles were used in subsequent experiments.

Compared with other MS preparation techniques such as inkjet printing, centrifugal sedimentation, and atomization methods, the AVIFJ in this study showed better consistency and biocompatibility and was particularly suitable for the continuous preparation of biomaterial MSs. Customized nozzles with adjustable diameters enable the printing of MSs with good shape controllability. When printing 2% sodium alginate, nozzles of different diameters can be applied to achieve a controllable adjustment of the MSs' diameter within 100–200 μm (Fig. 2). The parameterized printing process ensured good repeatability. The adjustable vibration amplitude and vibration period regulated the driving forces, avoided satellite micro-drops, and ensured high consistency of the printing process. However, the acceleration and maximum displacement generated by the piezoelectric ceramic were relatively limited, resulting in bio-inks with viscosities below 20 mPa·s. Finally, the printing process avoids the conditions of intense force, high heat, electric field, and UV light, and is therefore conducive for maintaining the original physicochemical properties of the printed biomaterial. When the hydrogel material contains cells, the preparation process can minimize the damage caused to the cells by driving forces.

3.2. Characterization of microcapsules and liquefied core

To mimic the microstructure of human alveoli, a shell structure with multiple layers and a liquefied core were successively constructed based on the printed MSs. Considering the polyanionicity of alginate hydrogel, a polycationic chitosan solution was adopted as a neutralizer for the coalescence effect. The illustration and actual results of the shells constructed by layer-by-layer condensation are shown in Figs. 3(a) and (b). The constructed 230 μm alginate hydrogel MSs were alternately coated with chitosan and sodium alginate solutions to form a microcapsule shell with a thickness of 4.152 ± 0.388 μm, as shown in Fig. 3(c). After core liquefaction, the permeability of the microcapsules was further revealed by the loss of red fluorescent particles, as shown in Fig. 3(b). The dynamic observation results in Fig. 3(d) show the obvious displacement of some fluorescent particles, proving that the core inside the microcapsule was liquefied.

A stable microcapsule structure was constructed to better biomimetic *in vivo* vesicular alveoli using the layer-by-layer coalescence technique. This method enabled the controlled construction of thin-shell structures from the nanometer to the micrometer scale by varying the polymer concentration and immersion time. In addition, coacervation-based microencapsulation and core liquefaction were both carried out under mild conditions and did not produce toxic residues, making them suitable for subsequent operations. The visible shell structure under the light microscope also demonstrated good microcapsule stability, providing solid support for cell adhesion and spatial tissue formation. Meanwhile, the semi-permeability of microcapsules also made it possible to further simulate the material exchange and air-liquid interface in the alveoli. Finally, the construction process and microcapsule structure provided additional ideas and references for the preparation of other vesicle structures, including kidney tubules and mammary glands.

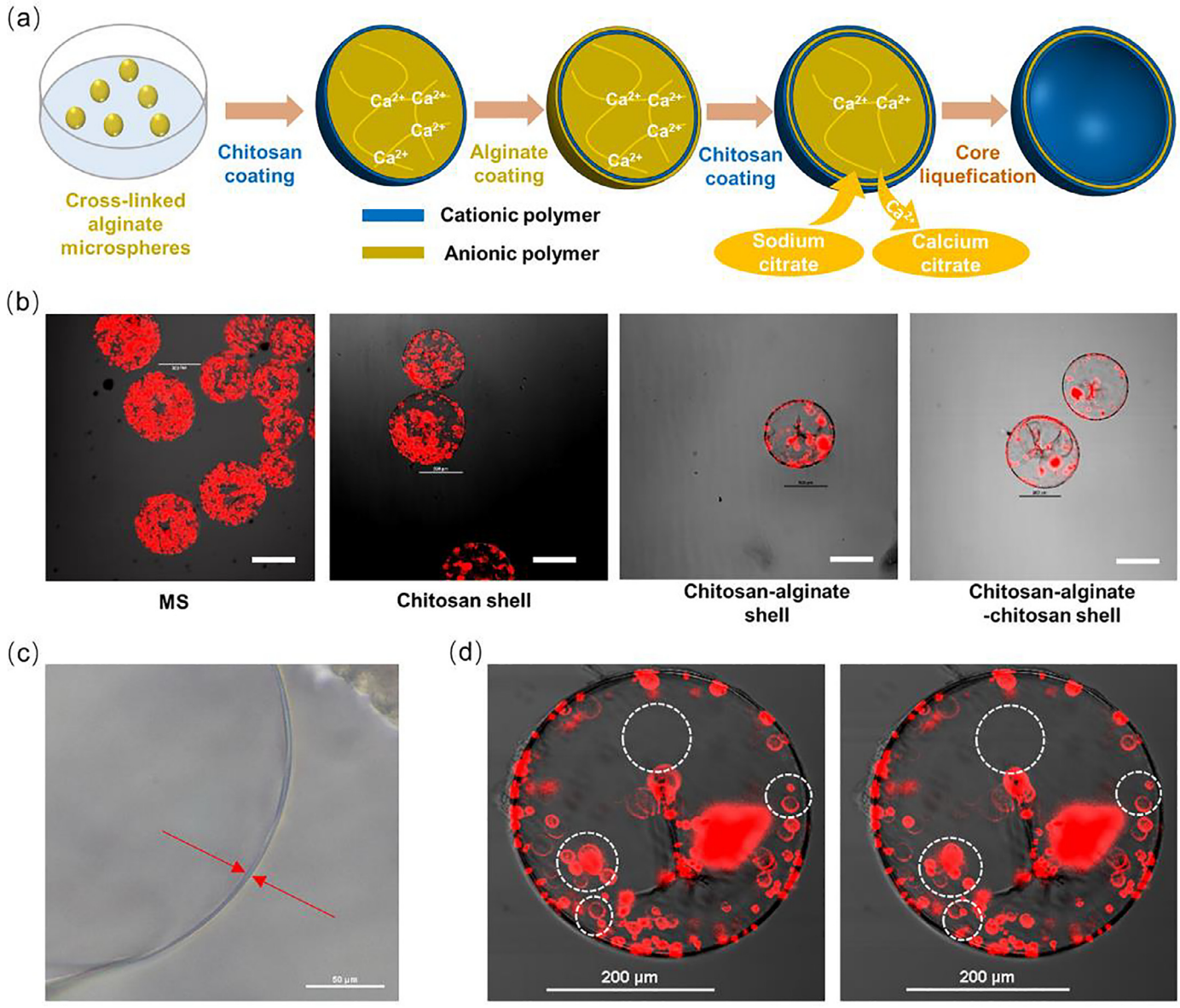

Fig. 3. Microencapsulation and core liquefication of alginate MS: (a) Route of layer-by-layer microencapsulation to form microcapsules with a shell of three layers (chitosan-alginate-chitosan) and its core liquefication; (b) Structure of MS after every step of microencapsulation (Scale bar: 200 μm); (c) Three-layer shell of microcapsule pointed by red arrows (Scale bar: 50 μm); (d) Displacement of red fluorescent particles in liquefied core of microcapsule (more obviously in the white circles) at an interval of 5 s.

3.3. Effects of different surface treatments on cell adhesion to microcapsules

To enhance cell adhesion to microcapsules, collagen, chitosan, polylysine, and different surface treatment processes were optimized in this study. The adhesion of cells on the surfaces of various microcapsules on the first and fifth days is shown in Fig. 4. Initially, the cells showed optimal adhesion on polylysine-treated microcapsules on day 1 (Fig. 4(d)). With increasing culture days, the cells showed optimal proliferation and adhesion on collagen-treated microcapsules on day 5, almost covering the entire surface (Fig. 4(a)). Meanwhile, the number of cells adhering to the polylysine-treated microcapsules on the fifth day was less than that on the first day. Therefore, coating a mixture of alginate and collagen onto the microcapsule surface was selected as the surface treatment for constructing the alveolar model.

The effects of the different materials and treatments on cell adhesion and proliferation were investigated and compared. Polylysine is a cationic polymer, and its strong electrostatic interaction with cells led to optimal cell adhesion on the first day. However, the cytotoxicity of unbound polylysine hindered cell proliferation on the microcapsules in the subsequent culture. By contrast, collagen facilitates cell adhesion by providing abundant surface receptors and better biocompatibility, leading to a weaker initial adhesion capacity but better cell proliferation. Furthermore, the collagen-alginate interpenetrating network structure (Fig. 4(a)) showed better cell adhesion and proliferation results than the collagen-coated structure (Fig. 4(b)), indicating that mixing is beneficial for cell encapsulation. The hybrid treatment process was assumed to form a tighter alginate-collagen linkage, providing a stronger adhesion site for the cells on the microcapsules in the dynamic culture environment instead of being washed off in the stepwise treatment procedure.

3.4. Multicellular distribution on the alveolar model

After co-culturing for 1 day, A549, HUVEC, and 3T3 cells adhered strongly to the curved surface of the microcapsules. The live/dead staining results revealed good cell survival of cells adhering to the surface of

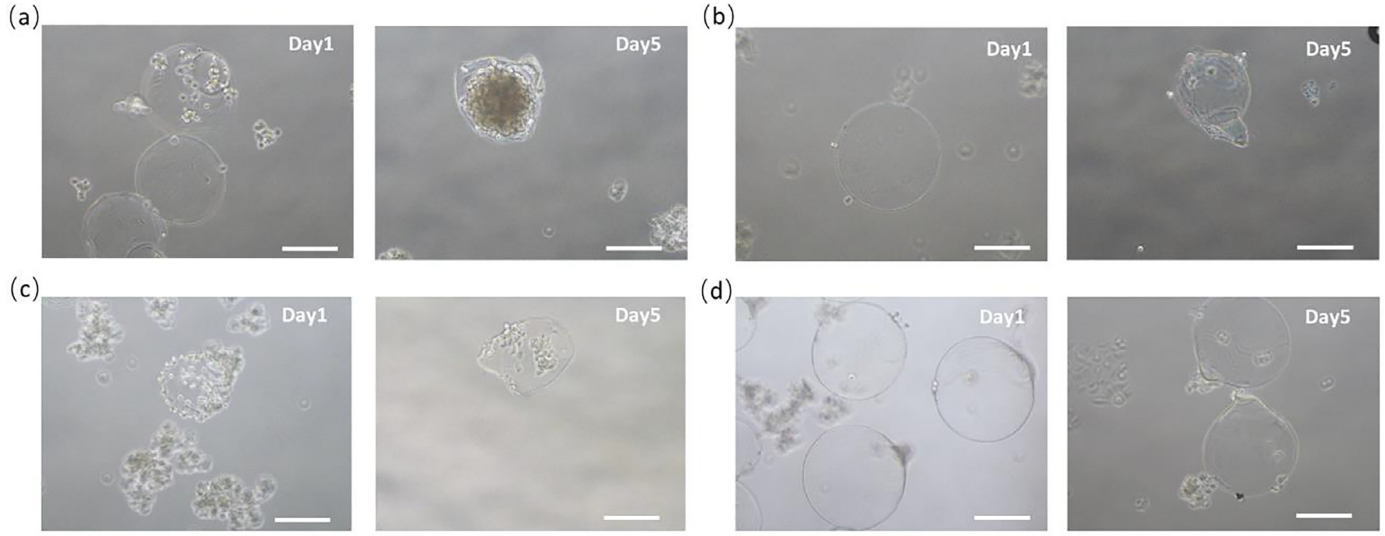

Fig. 4. Adhesion of A549 cells to microcapsules on day 1 and day 5 under different surface treatment: (a) Coating the mixture of alginate and collagen to the MS surface; (b) Coating alginate firstly then collagen; (c) Coating alginate firstly then chitosan; (d) Alginate firstly then polylysine (Scale bar: 200 μm).

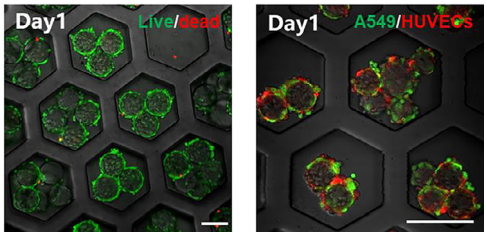

Fig. 5. Cellular distribution and live/dead staining assay of multiple cell-laden microcapsules on day 1 (Scale bar: 200 μm).

the microvesicles (Fig. 5). By comparing the area of green fluorescence with that of red fluorescence, the cell survival rate in the model reached 99.02% ± 1.01%.

The good cell adhesion and high survival rates verified the feasibility and potential application of this method in the construction of alveolar models. In the body, alveolar epithelial cells connect to form the alveolar wall, and are tightly connected to a rich capillary network. Thus, conventional models containing only single epithelial cells cannot fully reproduce intra-alveolar interactions [40]. The model developed in this study achieved the co-culture of three types of cells, which were expected to provide a richer intercellular matrix and tighter cell connections, thereby realizing advances in cell composition. In addition, there is growing evidence that the curvature of structures has an impact on cell expression, cyst formation and function [30,41,42]. Existing microfluidic chips and transwell technologies have achieved a controlled arrangement of multiple cells on a flat surface. The construction of an alveoli-like curved surface and realization of cell adhesion remain a challenge in the construction of *in vitro* models. The alveolar model developed in this study improved biomimetics by reproducing real alveolar size, curvature, and cell adhesion. Finally, this alveolar model can achieve cell adhesion within one day, shorten the preparation cycle, and facilitate mass production for toxicological assay applications.

3.5. Toxicity tests of glutaraldehyde

The cell survival rates of the alveolar model were 99.02% ± 1.01%, 90.62% ± 1.55%, 80.13% ± 4.63%, 48.74% ± 8.93%, 30.13%± 4.55%, and 13.98% ± 5.66% after treatment with 0, 100, 200, 400, 500, and 750 ng/mL glutaraldehyde, respectively, for 4 h. The fitting curve and half-lethal dose of inhalation (LD_{50}) of toxicity are shown in Fig. 6. The LD_{50} value of glutaraldehyde obtained in this model was 387.37 ng/mL,

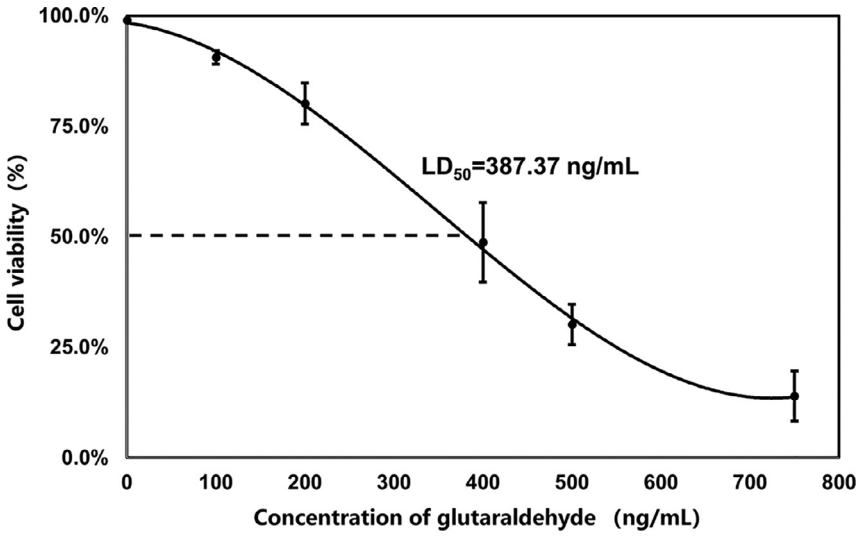

Fig. 6. Cytotoxic response curve to glutaraldehyde in the alveolar model.

which is in good agreement with the toxicity assessment of glutaraldehyde by the United States Environmental Protection Agency.

Glutaraldehyde is harmful via respiratory intake and can cause respiratory allergies, inhalation respiratory irritation, and occupational asthma. It is classified as a class II toxic substance by the US Environmental Protection Agency, and the LD_{50} for 4 h is between 50 and 500 ng/mL. The LD_{50} value obtained from the toxicity evaluation of glutaraldehyde based on the constructed model was in good agreement with the reference data, demonstrating the biomimetics of the model and its potential applications in toxicological evaluation (Fig. 6).

To provide more reliable models for toxicity tests, a novel alveolar model was constructed using 3D printing technology and sacrificial materials. This construction process overcomes the drawbacks of the long preparation cycle and low reproducibility of traditional animal models, providing a potential solution for high-throughput clinical needs. The constructed model further reproduced the 200 μm vesicle-like structure and achieved adhesion of multiple cell types to the curved surface, greatly improving the model's biomimetics and accuracy of toxicity test results. In follow-up work, we propose the construction of biomimetic alveoli containing pneumocytes, hierarchical cell distribution, and air-blood barriers. Gas diffusion assays will be carried out by adding gas-carrying microbubbles to the liquefied core. Controlled assembly of the alveolar model would be carried out to realize the *in vitro* construction of the bronchi structure, achieving progress from the alveolar model to the lung model. Finally, the model will be further applied in the detection of toxic gases, hazardous liquids, or particulate aerosols to open up more space for model applications.

4. Conclusions

This article proposed a research strategy for building alveolar models based on degradable hydrogel MSs to provide a more biomimetic platform for the future evaluation of toxicants and drugs. Alginate MSs with diameters of approximately 230 μm were obtained using 3D printing technology driven by AVIFJ. The mild layer-by-layer coalescence technique and core liquefaction realized the construction of the shell and liquefaction core of hydrogel microcapsules, respectively. The optimized surface treatment process promoted the initial adhesion and subsequent proliferation of cells on the 3D curved surfaces. Finally, an alveolar model containing an alveoli-like microcapsule structure, multiple cellular types, and 3D curved surfaces was constructed and proven to provide highly consistent results with reference data in the LD50 values of glutaraldehyde, demonstrating the potential applications of the current model in toxicity tests.

Declaration of Competing Interest

The authors declare that they have no known competing financial interests or personal relationships that could have influenced the work reported in this paper.

CRediT authorship contribution statement

Tiankun Liu: Methodology, data curation, formal analysis. **Chang Zhou:** Methodology, data curation, formal analysis. **Yongchun Shao:** Methodology, data curation, formal analysis. **Zhuo Xiong:** Validation, writing review & editing. **Ding Weng:** Methodology, resources, validation, writing review & editing. **Yuan Pang:** Methodology, resources. **Wei Sun:** Validation, writing review & editing.

Acknowledgments

This work was supported by Beijing Municipal Natural Science Foundation of China (Grant No. 3212007), Tsinghua University Spring Breeze Fund (Grant No. 20201080760), Tsinghua University Initiative Scientific Research Program (Grant No. 20213080030), National Key Research and Development Program of China (Grant No. 2018YFA0703004), National Natural Science Foundation of China (Grant No. 52175273), and 111 Project (Grant No. B17026).

References

[1] Massaro G D, Massaro D. Formation of pulmonary alveoli and gas-exchange surface area: Quantitation and regulation. Annu. Rev. Physiol. 1996;58(1):73–92.
[2] Roan E, Waters C M. What do we know about mechanical strain in lung alveoli? Am. J. Physiol. Lung Cell Mol. Physiol. 2011;301(5):L625–35.
[3] Rahaghi F N, Argemí G, Nardelli P, et al. Pulmonary vascular density: Comparison of findings on CT imaging with histology. Eur. Respir. J. 2019;54(2):1900370.
[4] Gutierrez G. Baum's textbook of pulmonary diseases. 7th ed. Baum's Textbook of Pulmonary Diseases; 2005.
[5] Sundarakrishnan A, Chen Y, Black L D, et al. Engineered cell and tissue models of pulmonary fibrosis. Adv. Drug Deliv. Rev. 2017:79–92.
[6] de Oliveira M, De Sibio M T, Costa F A S, et al. Airway and alveoli organoids as valuable research tools in COVID-19. ACS Biomater. Sci. Eng. 2021;7(8):3487–502.
[7] Tian L, Gao J, Garcia I M, et al. Human pluripotent stem cell-derived lung organoids: Potential applications in development and disease modeling. Wiley Interdiscip. Rev. Dev. Biol. 2021;10(6):e399.
[8] Asba B, Ac C, Bsab D. Building three-dimensional lung models for studying pharmacokinetics of inhaled drugs. Adv. Drug Deliv. Rev. 2021;170:386–95.
[9] Peter J. Barnes. Targeting cytokines to treat asthma and chronic obstructive pulmonary disease. Nat. Rev. Immunol. 2018.
[10] Pippin J J. Animal research in medical sciences: Seeking a convergence of science, medicine and animal law. S. Tex. L. Rev 2012;18:454–66.
[11] Wu J, Wang Y, Liu G, et al. Characterization of air-liquid interface culture of A549 alveolar epithelial cells. Braz. J. Med. Biol. Res. 2018;51(2):e6950.
[12] Ziókowska K, Kwapiszewski R, Brzózka Z. Microfluidic devices as tools for mimicking *in vivo* environment. N. J.Chem. 2011;35(5):979–90.
[13] Hilton G, Barosova H, Petri-Fink A, et al. Leveraging proteomics to compare submerged *versus* air-liquid interface carbon nanotube exposure to a 3D lung cell model. Toxicol. in Vitro: Int. J. Publ. Assoc. BIBRA 2019;54:58–66.
[14] Bisig C, Voss C, Petri-Fink A, et al. The crux of positive controls - Pro-inflammatory responses in lung cell models. Toxicol. in Vitro 2018;54:189–93.
[15] Neilson L, Mankus C, Thorne D, et al. Development of an *in vitro* cytotoxicity model for aerosol exposure using 3D reconstructed human airway tissue; application for assessment of e-cigarette aerosol. Toxicol. in Vitro 2015;29(7):1952–62.
[16] Kang D, Ju A P, Kim W, et al. All-inkjet-printed 3D alveolar barrier model with physiologically relevant microarchitecture. Adv. Sci. 2021;8(10):2004990.
[17] Crapo P M, Gilbert T W, Badylak S F. An overview of tissue and whole organ decellularization processes. Biomaterials 2011;32(12):3233–43.
[18] Gilpin S E, Wagner D E. Acellular human lung scaffolds to model lung disease and tissue regeneration. Eur. Respir. Rev. 2018;27(148):180021.
[19] Zhang B, Anastasia K, Lai B, et al. Advances in organ-on-a-chip engineering. Nat. Rev. Mater. 2018;3:257–78.
[20] Wang Z, Samanipour R, Kim K. Organ-on-a-chip platforms for drug screening and tissue engineering. Springer International Publishing; 2016.
[21] Ghaemmaghami A M, Hancock M J, Harrington H, et al. Biomimetic tissues on a chip for drug discovery. Drug Discov. Today 2012;17(3–4):173–81.
[22] Huh D, Hamilton G A, Ingber D E. From 3D cell culture to organs-on-chips. Trends Cell Biol. 2011;21(12):745–54.
[23] Huh D, Matthews B D, Mammoto A, et al. Reconstituting organ-level lung functions on a chip. Science 2010;328(5986):1662–8.
[24] Zhang M, Wang P, Luo R, et al. Biomimetic human disease model of SARS–CoV-2 induced lung injury and immune responses on organ chip system. Adv. Sci. 2021;8(3):2002928.
[25] Zhang B, Radisic M. Organ-on-a-chip devices advance to market. Lab Chip 2017:10–1039.
[26] Zhang F, Liu W, Zhou S, et al. Investigation of environmental pollutant-induced lung inflammation and injury in a 3D coculture-based microfluidic pulmonary alveolus system. Anal. Chem. 2020;92(10):7200–8.
[27] Lan Ca Ster M A, Knoblich J A. Organogenesis in a dish: Modeling development and disease using organoid technologies. Science 2014;345(6194):1247125.
[28] Dutta D, Heo I, Clevers H. Disease modeling in stem cell-derived 3D organoid systems. Trends Mol. Med. 2017;23(5):393.
[29] Galliger Z, Vogt C D, Panoskaltsis-Mortari A. 3D bioprinting for lungs and hollow organs. Trans. Res. 2019;211:19–34.
[30] Baptista D, Teixeira L, Blitterswijk C V, et al. Overlooked? Underestimated? Effects of substrate curvature on cell behavior. Trends Biotechnol. 2019;37(8):838–54.
[31] Callens S, Uyttendaele R, Fratila-Apachitei L E, et al. Substrate curvature as a cue to guide spatiotemporal cell and tissue organization. Biomaterials 2019;232:119739.
[32] Baptista D, Teixeira L M, Birgani Z T, et al. 3D alveolar *in vitro* model based on epithelialized biomimetically curved culture membranes. Biomaterials 2021;266:120436.
[33] Wei L N, Ayi T C, Liu Y C, et al. Fabrication and characterization of 3D bioprinted triple-layered human alveolar lung models. Int. J. Bioprinting 2022;7(2):53–67.
[34] Foster K A, Avery M L, Yazdanian M, et al. Characterization of the Calu-3 cell line as a tool to screen pulmonary drug delivery. Int. J. Pharm. 2000;208(1–2):1–11.
[35] Weibel E R. It takes more than cells to make a good lung. Am. J. Respir. Crit. Care Med. 2013;187(4):342–6.
[36] Liu T, Shao Y, Wang Z, et al. 3D printing of *in vitro* hydrogel microcarriers by alternating viscous-inertial force jetting. J. Vis. Exp.: JoVE 2021(170). doi:10.3791/62252.
[37] Liu T K, Pang Y, Zhou Z Z, et al. An integrated cell printing system for the construction of heterogeneous tissue models. Acta Biomater. 2019;95:245–57.

[38] Pang Y, Montagne K, Shinohara M, et al. Liver tissue engineering based on aggregate assembly: Efficient formation of endothelialized rat hepatocyte aggregates and their immobilization with biodegradable fibres. Biofabrication 2012;4(4):45004.
[39] He J, Pang Y, Yang H, et al. Modular assembly–based approach of loosely packing co-cultured hepatic tissue elements with endothelialization for liver tissue engineering. Ann. Transl. Med. 2020;8(21):1400.
[40] Choi C, Weitz D A, Lee C. One step formation of controllable complex emulsions: From functional particles to simultaneous encapsulation of hydrophilic and hydrophobic agents into desired position. Adv. Mater. 2013;25(18):2536–41.
[41] Lewis K J R, Tibbitt M W, Zhao Y, et al. *In vitro* model alveoli from photodegradable microsphere templates. Biomater. Sci. 2015;3(6):821–32.
[42] Callens S J P, Uyttendaele R J C, Fratila-Apachitei L E, et al. Substrate curvature as a cue to guide spatiotemporal cell and tissue organization. Biomaterials 2020;232:119739.